We are IntechOpen, the world's leading publisher of Open Access books Built by scientists, for scientists

4,800
Open access books available

122,000
International authors and editors

135M
Downloads

Our authors are among the

154
Countries delivered to

TOP 1%
most cited scientists

12.2%
Contributors from top 500 universities

CLARIVATE ANALYTICS BOOK CITATION INDEX INDEXED

WEB OF SCIENCE™

Selection of our books indexed in the Book Citation Index in Web of Science™ Core Collection (BKCI)

Interested in publishing with us?
Contact book.department@intechopen.com

Numbers displayed above are based on latest data collected.
For more information visit www.intechopen.com

11

Applying Estimation Techniques to Chaos-based Digital Communications

Marcio Eisencraft[1] and Luiz Antonio Baccalá[2]
[1]*Centro de Eng., Modelagem e Ciências Sociais Aplicadas, Universidade Federal do ABC*
[2]*Escola Politécnica da Universidade de São Paulo*
Brazil

1. Introduction

Chaotic signal applications have been considered in a variety of areas, see e.g. (Strogatz, 2001). Signal Processing and Telecommunications are no exception specially after the seminal work by Pecora & Carroll (1990). Applications of chaos ranging from digital and analog modulation to cryptography, pseudorandom sequences generation and watermarking have been proposed (Kennedy & Kolumban, 2000; Kennedy, Setti & Rovatti, 2000; Stavroulakis, 2005; Tsekeridou et al., 2001). Chaos has also been shown in connection to devices used in signal processing such as nonlinear adaptive filters and phase-locked loop networks (Endo & Chua, 1988; Harb & Harb, 2004; Monteiro et al., 2009; Tavazoei & Haeri, 2009).

In particular, many recent works have described digital modulations using chaotic carriers (Kennedy & Kolumban, 2000; Kennedy, Setti & Rovatti, 2000; Kolumban et al., 1997; Kolumban, Kennedy & Chua, 1998; Lau & Tse, 2003) even though their performance proved below that of equivalent conventional systems under additive white gaussian noise channel (Kaddoum et al., 2009; Williams, 2001).

This chapter's first aim is to compare these chaos-based modulations to their conventional counterparts via their discrete-time low-pass equivalent models. Special attention is devoted to Chaos Shift Keying (CSK), Differential CSK and some of their variants in Section 3 as that analysis points out reasons for the low observed performance of chaotic modulation and thus paves the way for result improvement.

In fact, we show that the poor Bit Error Rate (BER) performance of many current modulations employing chaos is in part due to their systematic neglect of the details behind the chaos generation mechanisms. To overcome this we explicitly exploit chaos generating map information to estimate the received noise-embedded chaotic signal (Section 4) and show that it leads to improved BER performance. Two approaches to achieve that are considered and contrasted: (a) Maximum Likelihood Estimation and (b) the Modified Viterbi Algorithm (MVA) for discrete-time one-dimensional chaotic maps.

In the context of MVA, we further examine two digital modulation schemes: the Modified Maximum Likelihood Chaos Shift Keying using (a) one and (b) two maps both of which have better BER characteristics than previous noncoherent chaos communication schemes (Section 5).

Before proceeding we start reviewing basic definitions and the discrete-time low-pass equivalent models.

2. Preliminary notions

For our present purposes we take a limited signal to be chaotic if it is deterministic, aperiodic and exhibits sensitive dependence on initial conditions (Alligood et al., 1997), i.e. when its generating system is initialized in a slightly different initial condition, the resulting signal very quickly diverges from that with the original unperturbed initial conditions.
Due to these properties, chaotic signals occupy a large bandwidth, their autocorrelations are impulsive and the cross-correlations between signals generated by different initial conditions present low values (Djurovic & Rubezic, 2008; Kennedy & Kolumban, 2000; Kennedy, Setti & Rovatti, 2000; Stavroulakis, 2005). These characteristics have been behind the rationale for using chaotic signals as candidates for spreading signal information. When chaotic signals modulate independent narrowband sources increased bandwidths result with lower power spectral density levels in a fashion similar to what happens in Spread Spectrum (SS) systems (Lathi, 1998). Consequently, chaos-based and SS systems share several properties namely (i) they are difficult to intercept by any unauthorized user; (ii) they are easily hidden, i.e. from any unauthorized receiver, it is difficult to even detect their presence in many cases; (iii) they are resistant to jamming; and (iv) they provide a measure of immunity to distortion due to multipath propagation.
The unified low pass representation used here is based on (Kolumban et al., 1997; Kolumban, Kennedy & Chua, 1998) in the discrete time context which is more suitable to treating signals generated by chaotic maps.
In the following, only the transmission of isolated symbols is considered, i.e. intersymbol interference is assumed absent.

2.1 Equivalent low-pass discrete-time models

To facilitate simulation and analysis of digital modulations it is usual to work with discrete-time baseband equivalent models, whose results are valid for the original ones (Lathi, 1998). This modeling allows us to represent the transmitted signals by means of finite length sequences.
In the conventional case, a baseband signal, supposed to have a bandwidth B, is used to modify the sinusoidal carrier with frequency $f_0 \gg B$.
As any bandpass signal can be described by (Lathi, 1998)

$$x(t) = x_c(t)\cos(2\pi f_0 t) - x_s(t)\sin(2\pi f_0 t), \tag{1}$$

its low-pass representation denoted by $x_l(t)$ turns out to be a complex function with real and imaginary parts $x_c(t)$ and $x_s(t)$ respectively, so that:

$$x_l(t) = x_c(t) + jx_s(t), \tag{2}$$

where both $x_c(t)$ and $x_s(t)$ are low-pass signals termed *in-phase* and *quadrature* components respectively (Haykin, 2000).
The discrete-time version of the baseband model is obtained sampling $x_l(t)$ at a convenient sampling rate $1/T_A$ (Lathi, 1998). To simplify the notation, we denote $x_l(nT_a)$ as $x(n)$.
The set of equivalent waveform sequences used in a given system using M symbols is represented by $x_m(n)$, $m = 1, 2, \ldots, M$, where $x_m(n) \neq 0$ only for $0 \leq n \leq N-1$. To transmit the m-th symbol, the signal represented in discrete-time by $x_m(n)$ is sent through the analog channel.

To simplify demodulation, it is convenient to define a set with fewer signals, called *basis functions*, so that the signals represented by $x_m(n)$ are weighted sums of the elements of this basis (Wozencraft & Jacobs, 1987).
Let $s_i(n)$, $i = 1, 2, \ldots, N_b$, $n = 0, 1, \ldots, N-1$ be an orthonormal basis sequence, i.e.,

$$\sum_{n=0}^{N-1} s_i(n)s_j(n) = \begin{cases} 1, & \text{if } i = j \\ 0, & \text{if } i \neq j \end{cases}, 1 \leq i, j \leq N_b. \tag{3}$$

Thus, each of the M signals $x_m(n)$ is represented as a linear combination of the N_b sequences $s_i(n)$, with $N_b \leq M$:

$$x_m(n) = \sum_{i=1}^{N_b} x_{mi}s_i(n),\ m = 1, 2, \ldots, M. \tag{4}$$

The coefficients x_{mi} in Eq.(4) can be interpreted as the components of an N_b-dimensional column vector $\mathbf{x}_m$.
Since the basis sequences are orthonormal, the $\mathbf{x}_m$ signal vector can be recovered from the transmitted signal if all basis signals $s_i(n)$ are known:

$$x_{mi} = \sum_{n=0}^{N-1} x_m(n)s_i(n),\ i = 1,\ 2,\ \ldots,\ N_b. \tag{5}$$

Interestingly, this notation applies to both conventional and chaotic modulations. The difference between them lies in the nature of the chosen basis.
The chaotic sequences in the next section are assumed to be composed of N points derived from the tent map $f_T(.)$ defined by

$$s(n+1) = f_T\left(s(n)\right) = 1 - 2\left|s(n)\right|,\ 0 \leq n \leq N-1, \tag{6}$$

with initial conditions $s(0)$ uniformly distributed over the $(-1, 1)$ interval. To achieve unit mean energy the latter sequences are then multiplied by $\sqrt{3/N}$ (Eisencraft et al., 2010).

3. Digital modulations using chaotic carriers

We focus on Chaos Shift Keying (CSK) and its variants based on noncoherent or differential demodulation because of their promise in proposed practical applications (Kennedy, Kolumbán, Kis & Jákó, 2000; Kennedy, Setti & Rovatti, 2000; Kolumban et al., 1997; Kolumban, Kennedy & Chua, 1998; Lau & Tse, 2003; Stavroulakis, 2005). In fact, researchers from the Optical Communications Laboratory of the Athens University in Greece, implemented an 120km optical fiber link in metropolitan Athens and managed to transmit at gigabit rates using CSK (Argyris et al., 2005; Syvridis, 2009).

3.1 The CSK and the DCSK

CSK is a digital modulation where each symbol to be transmitted is encoded as the coefficients of a linear combination of signals generated by different chaotic attractors (Kolumban et al., 1997).
Using the previously defined notation, the required basis sequences must be chosen as segments of the chaotic signals generated by N_b different attractors. As a result of the chaos related non-periodicity, the sequences $s_i(n)$ and therefore the signals $x_m(n)$ are different for each subsequent transmitted symbol.

We impose that the chaotic basis sequences are orthonormal *in the mean*, i.e.

$$E\left[\sum_{n=0}^{N-1} s_i(n)s_j(n)\right] = \begin{cases} 1, \text{ if } i = j \\ 0, \text{ if } i \neq j \end{cases}, \quad 1 \leq i,j \leq N_b, \tag{7}$$

where $E[.]$ denotes the expectation operator. Eq.(7) identifies an important characteristic of digital chaotic modulation schemes: the orthonormality of the basis signals can be defined only in terms of expected values.
Using Eq. (5), the coefficients x_{mi} can be recovered from the transmitted signal by correlation with locally generated copies of the basis sequences $\hat{s}_i(n)$ as shown in Figure 1(a) for the case $N_b = 1$.

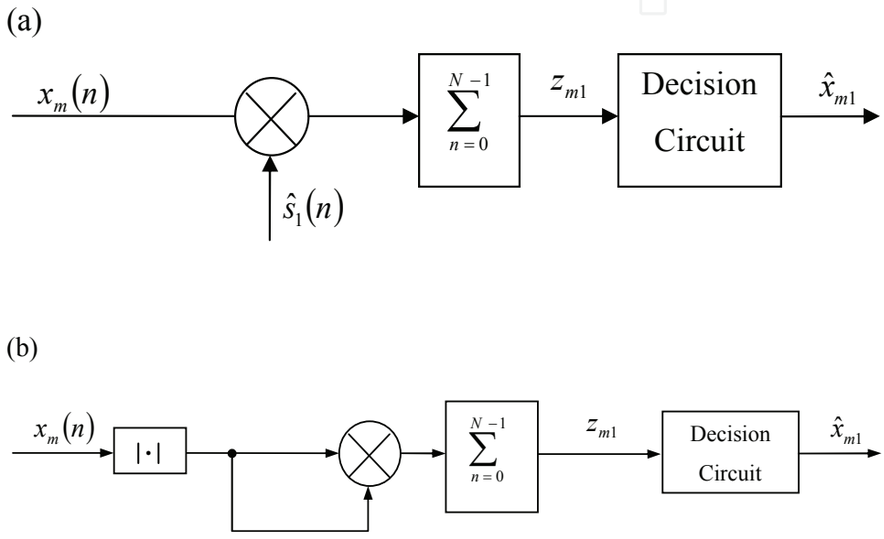

Fig. 1. Receiver (a) coherent and (b) non-coherent case with $N_b = 1$.

If the coefficients x_{mi} generate signals with different energies for each m, demodulation can also be done by estimating the energy of the received signal. In this case, copies of the basis sequences are unnecessary. A block diagram of the non-coherent demodulator for $N_b = 1$ is shown in Figure 1(b).
In the special case of binary CSK with one basis function, the symbols are transmitted using the signals $x_1(n) = x_{11}s_1(n)$ and $x_2(n) = x_{21}s_1(n)$. Three possibilities are highlighted in the literature:

i. **Unipodal CSK** (Kennedy, Setti & Rovatti, 2000), where x_{11} and x_{21} are positive and different;

ii. **Chaotic On-Off Keying (COOK)** (Kolumban, Kennedy & Chua, 1998), where x_{11} is positive and $x_{21} = 0$ and

iii. **Antipodal CSK**(Kennedy, Setti & Rovatti, 2000), where $x_{21} = -x_{11} \neq 0$.

Figure 2 shows examples of transmitted signals $x(n)$ for the sequence of symbols $\{1,1,0,1,0,0,1,0\}$ using each type of CSK above, with $N = 50$ and mean energy per symbol $E_b = 1$. The $s_1(n)$ sequence is obtained by iterating the tent map of Eq. (6). The symbols "1" and "0" are transmitted using $x_1(n) = x_{11}s_1(n)$ and $x_2(n) = x_{21}s_1(n)$ respectively.

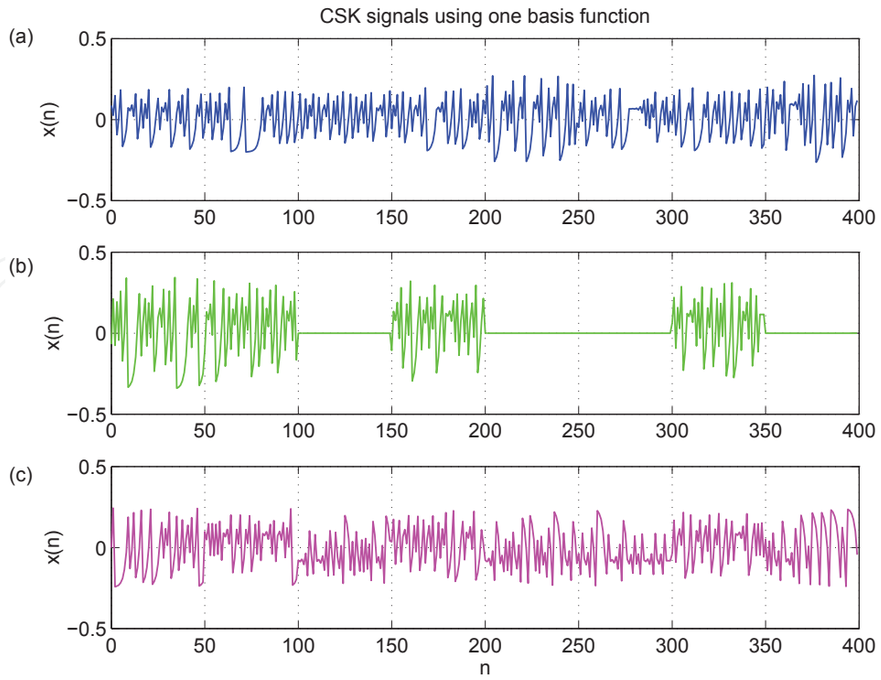

Fig. 2. CSK transmitted signals for the sequence $\{1,1,0,1,0,0,1,0\}$: (a) unipodal CSK; (b) COOK; (c) antipodal CSK. In each case, $N = 50$ samples and $E_b = 1$.

Differential CSK (DCSK) is a variant of CSK with two maps whose basis sequences consist of repeated segments of chaotic waveforms. For DCSK the two basis signals are chosen as:

$$s_i(n) = \begin{cases} s(n), & 0 \leq n < \frac{N}{2} \\ (-1)^{i+1} s\left(n - \frac{N}{2}\right), & \frac{N}{2} \leq n < N \end{cases}, \tag{8}$$

where $i = 1, 2$, $s(n)$ is a chip of a chaotic signal and N is even.
A typical binary DCSK signal $x(n)$ corresponding to the symbol sequence $\{1,1,0,1,0,0,1,0\}$ using the tent map $f_T(.)$ from Eq. (6) as the chaotic generator is shown in Figure 3. Symbols "1" and "0" are transmitted using $x_1(n) = \sqrt{E_b} s_1(n)$ and $x_2(n) = \sqrt{E_b} s_2(n)$ respectively. The number of samples per symbol is $N = 50$ and $E_b = 1$.

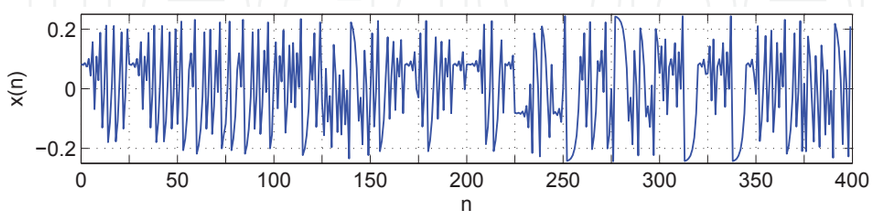

Fig. 3. DCSK signal transmitted for the data sequence $\{1,1,0,1,0,0,1,0\}$ with $N = 50$ samples and $E_b = 1$.

In the DCSK signal, information is mapped on the correlation between the *reference chip* $(0 \leq n < N/2)$ and the *information-bearing chip* $(N/2 \leq n < N)$. Thus, one may demodulate the signal with a differential receiver, besides the coherent correlation receiver (Lathi, 1998).

The block diagram of a differential DCSK receiver is shown in Figure 4. The received signal is delayed by $N/2$, half of its duration and the correlation between the received signal and its delayed version is determined. The observation variable z_{m1} is obtained by sampling the output of the correlator at time $(N-1)$.

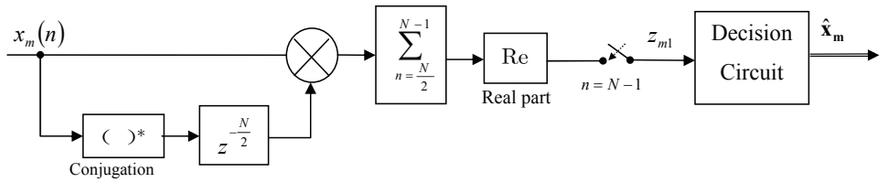

Fig. 4. Block diagram of a differential DCSK receiver.

3.2 The energy per symbol variability problem and FM-DCSK

For a conventional modulation scheme using only one periodic basis function $s_1(n)$ composed of N samples per symbol as an integer multiple of the period of $s_1(n)$, the energy per symbol is given by

$$E_{bm} = x_{m1}^2 \sum_{n=0}^{N-1} s_1^2(n) \tag{9}$$

and is constant for each distinct symbol. In contrast, chaotic signals are by definition aperiodic. Thus, when using a chaotic basis, $s_1(n)$ is different at each interval and

$$E_{s1} = \sum_{n=0}^{N-1} s_1^2(n) \tag{10}$$

is different for each transmitted symbol.

In the periodic case, all values of E_{s1} are equal to $\sum_{n=0}^{N-1} s_1^2(n)$ with zero variance. In the chaotic case, the values of E_{s1} are centered at $E\left[\sum_{n=0}^{N-1} s_1^2(n)\right]$ with non-zero variance.

Compared to conventional systems, the fact that the energy per symbol is not constant is a major disadvantage of the communication systems using chaotic signals discussed so far. For them, errors in reception can occur even in ideal noiseless channels, which is undesirable in practice. Increasing the number of points N does not solve the problem as the standard deviation in the estimate of E_{s1} falls slowly with N (Kennedy, Setti & Rovatti, 2000). Furthermore increasing the number of transmitted points per symbol also limits the maximum transmission rate.

An alternative solution is to modify the modulation scheme so that the transmitted energy for each symbol is kept constant. That is the aim of Frequency Modulated DCSK (FM-DCSK) (Kolumbán, Kennedy, Kis & Jákó, 1998).

The FM-DCSK transmitter generates a DCSK signal with constant energy per symbol. The idea is to take advantage of the fact that the power of a frequency modulated signal is independent of the signal, as long as it is slowly-varying compared to the carrier (Lathi, 1998). Thus, the chaotic signal is fed into a frequency modulator. If the output of this modulator is used in implementing DCSK, then the output of the correlator at the receiver will be a constant in the absence of noise and the problem of energy variability disappears.

For its simulation and analysis, the equivalent discrete time low-pass model of the FM-DCSK may be obtained by considering a reference chip described by

$$x_m(t) = A\cos\left[2\pi\left(f_0 + K_f s(t)\right)t\right],\ 0 \le t < \frac{T}{2}, \tag{11}$$

where T is the symbol period, f_0 is the carrier frequency, A and K_f are constants (Lathi, 1998). The constant K_f that defines the modulation intensity is heretofore taken as 1. Hence, one can rewrite Eq. (11) as

$$x_m(t) = A\left[\cos(2\pi s(t)t)\cos(2\pi f_0 t) - \sin(2\pi s(t)t)\sin(2\pi f_0 t)\right], \tag{12}$$

with $0 \leq t \leq T/2$. Thus, according to Eq. (2), the discrete-time low-pass equivalent of this chip of $x_m(t)$ becomes

$$x_m(n) = A\left[\cos(2\pi s(n)n) + j\sin(2\pi s(n)n)\right] = Ae^{j2\pi n s(n)} \tag{13}$$

with $0 \leq n < N/2$, N even.
Note that $|x_m(n)| = A$ for any n. We adopt $A = \sqrt{\frac{E_b}{N}}$ so that each symbol is represented as a signal with energy E_b and

$$x_m(n) = \sqrt{\frac{E_b}{N}} e^{j2\pi n s(n)},\ 0 \leq n < N/2. \tag{14}$$

The information-bearing chip occupies the time slot $N/2 \leq n < N$ and repeats the reference chip for $m = 1$ or is equal to its opposite for $m = 2$.
A block diagram of a low-pass equivalent FM-DCSK signals generator is shown in Figure 5.

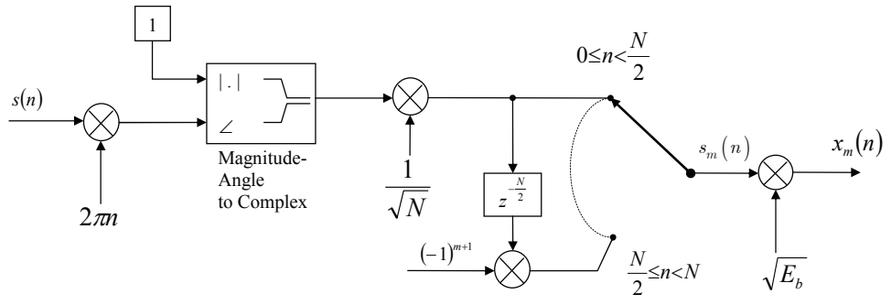

Fig. 5. Block diagram of a discrete-time FM-DCSK signals generator, $m = 1, 2$.

Figure 6 shows the real and imaginary part of the low-pass equivalent $x(n)$ of an FM-DCSK signal for the symbol sequence $\{1,1,0,1,0,0,1,0\}$ using $N = 50$ samples per symbol and $E_b = 1$. Again symbol "1" and "0" are transmitted using $x_1(n)$ and $x_2(n)$ respectively using iterations of Eq. (6) to generate $s(n)$.

3.3 Comparison of performance in AWGN channel

Next we consider the Additive White Gaussian Noise (AWGN) channel performance of the afore mentioned modulations. For simplicity, only binary transmission systems using a single basis sequence $s_1(n)$ are examined. As such the transmitted signals are $x_m(n) = x_{m1}s_1(n)$, $m = 1, 2$. We denote by $\hat{s}_1(n)$ the reference signal and by $x'_m(n)$ the noisy signal that arrives at the receiver:

$$x'_m(n) = x_m(n) + r(n) = x_{m1}s_1(n) + r(n), \tag{15}$$

where $r(n)$ is zero mean AWGN with power σ^2.

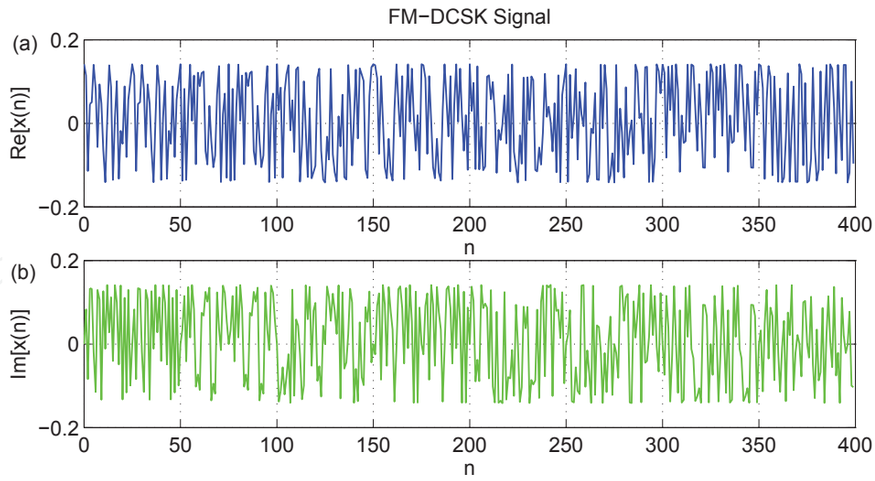

Fig. 6. (a) Real and (b) imaginary part of an FM-DCSK signal for the data sequence $\{1,1,0,1,0,0,1,0\}$ using $N = 50$ samples and $E_b = 1$.

3.3.1 Non-coherent correlation receiver

In a non-coherent correlation receiver, as shown in Figure 1(b), the reference signal $\hat{s}_1(n)$ is equal to the signal that reaches the receiver $x'_m(n) = x_m(n) + r(n)$ and the observed component can be expressed as

$$z_{m1} = \sum_{n=0}^{N-1} (x_m(n) + r(n))^2 = \sum_{n=0}^{N-1} x_m^2(n) + 2\sum_{n=0}^{N-1} x_m(n)r(n) + \sum_{n=0}^{N-1} r^2(n). \tag{16}$$

In the noiseless case, $r(n) = 0$ and the expected value of the observed component is equal to the mean energy of the transmitted symbol, x_{m1}^2.

The presence of noise in the channel causes the expected value of the random variable z_{m1} to differ from x_{m1}^2. The expected value of z_{m1} depends on the chaotic signal and on the noise power as expressed by the first and third terms of the right member of Eq. (16), respectively.

In this case, z_{m1} *is a biased estimator of the energy of* $x_m(n)$ *and the threshold used at the comparator decision circuit explicitly depends on the noise level*. The way to produce an unbiased estimator with larger distance between the observed component symbols is to use coherent CSK or DCSK.

3.3.2 Coherent correlation receiver with chaotic synchronization

Let $\hat{s}_1(n)$ be the chaotic basis function recovered so that $\hat{s}_1(n) \approx s_1(n)$ for $n \geq N_{Sync}$ in Figure 1(a).

One drawback of the coherent CSK receiver is that synchronization is lost and recovered each time a new symbol is transmitted (Kennedy, Setti & Rovatti, 2000). Thus, N_{Sync} samples of each symbol are required for synchronization. In other words synchronization time imposes an upper bound on the symbol rate and thus on the data rate.

As the synchronization transient can not be used to transmit information, the observed component is obtained by correlation only in the interval $N_{Sync} \leq n < N-1$. Let $x_m(n)$, $m = 1,2$, be the transmitted signals for the CSK binary modulation with a single basis

sequence $s_1(n)$. Then, the observed component is given by

$$z_{m1} = \sum_{n=N_{Sync}}^{N-1} [x_m(n) + r(n)]\,\hat{s}_1(n) = \sum_{n=N_{Sync}}^{N-1} [x_{m1}s_1(n) + r(n)]\,\hat{s}_1(n) =$$
$$= x_{m1} \sum_{n=N_{Sync}}^{N-1} s_1(n)\hat{s}_1(n) + \sum_{n=N_{Sync}}^{N-1} r(n)\hat{s}_1(n). \tag{17}$$

Assuming that $r(n)$ and $\hat{s}_1(n)$ are uncorrelated, the mean value of z_{m1} is independent of noise; thus, the receiver becomes an *unbiased estimator* of x_{m1}; in particular, the decision level in the comparator does not depend on the noise level in the channel.

As with conventional coherent receivers that use periodic basis functions, the performance of coherent receivers that use chaotic basis functions under AWGN is theoretically optimal (Lathi, 1998). However, the BER also depends on synchronization quality, i.e., the closeness between the reference signal $\hat{s}_1(n)$ and the original chaotic basis function $s_1(n)$. Any synchronization error, especially the loss of synchronization, leads to large performance degradation (Kennedy, Setti & Rovatti, 2000).

Chaos synchronization techniques published to date are very sensitive to noise. In particular, the basis functions $s_i(n)$ can not be recovered exactly when $x'_m(n) \neq x_m(n)$ (Kennedy, Setti & Rovatti, 2000; Williams, 2001). This makes receivers based on chaotic synchronization unsuitable for propagation environments with low SNR.

The number of samples N_{Sync} needed for synchronization is another factor that degrades the performance of these systems under noise. As no information can be transmitted during the synchronization transient, the energy corresponding to that signal section is lost implying BER degradation.

Thus, even though coherent correlation CSK receivers outperform non-coherent ones by providing an unbiased transmitted symbol estimator, its performance depends critically on the ability to regenerate the basis functions at the receiver. The existing chaotic synchronization techniques are insufficiently robust for practical wireless communication systems (Williams, 2001).

3.3.3 Differential receiver

In a differential receiver for DCSK or FM-DCSK, the reference signal $\hat{s}(n)$ is a delayed version of the noisy signal that reaches the receiver, as was shown in Figure 4. Note that different noise samples corrupt the correlator entries. The observed component is given by

$$z_{m1} = \sum_{n=\frac{N}{2}}^{N-1} [x_m(n) + r(n)] \left[x_m\left(n - \frac{N}{2}\right) + r\left(n - \frac{N}{2}\right) \right]. \tag{18}$$

Substituting Eqs.(4) and (8) in Eq.(18) gives the observed component for DCSK as

$$z_{m1} = (-1)^{m+1} E_b \sum_{n=\frac{N}{2}}^{N-1} s^2(n) + \sqrt{E_b} \sum_{n=\frac{N}{2}}^{N-1} r(n) s\left(n - \frac{N}{2}\right) + (-1)^{m+1} \sqrt{E_b} \sum_{n=\frac{N}{2}}^{N-1} s(n) r\left(n - \frac{N}{2}\right) +$$
$$\sum_{n=\frac{N}{2}}^{N-1} r(n) r\left(n - \frac{N}{2}\right), \tag{19}$$

assuming $s(n) = s\left(n - \frac{N}{2}\right)$ for $N/2 \leq n < N$.

For DCSK, the mean value of the first term is $E_b/2$ or $-E_b/2$. In the equivalent FM-DCSK case, the transmitted symbol energy value is constant and equal to $E_b/2$ or $-E_b/2$. The other three terms containing the AWGN sequence are zero mean. This shows that z_{m1} is an unbiased estimator of $\pm E_b/2$ in this case. The decision level is zero and independent of the noise level in the channel.

In the DCSK case, the variance of z_{m1} is determined by the statistical variability of the energy per symbol of the chaotic signal and by the noise power in the channel. Therefore, the uncertainty in the energy estimation also influences the performance of DCSK.

For the FM-DCSK, the first term of Eq.(19) equals $\pm E_b/2$ and the uncertainty in the energy estimation does not appear, also the decision threshold is fixed and there is no need for chaotic synchronization. This makes FM-DCSK superior to the other previous chaotic modulations schemes in terms of performance in AWGN channel.

In Figure 7 we numerically evaluate the performance of the analyzed systems in terms of BER as a function of E_b/N_0 for $N = 10$. The white noise power spectral density in the channel is $N_0/2$. As expected, it is clear that the FM-DCSK is the one that has the best performance among them. This is so basically because the energy per symbol is kept constant in this system. Still, its performance is below that of its counterpart using sinusoidal carriers, the Differential Phase Shift Keying (DPSK). In DPSK the knowledge of the basis functions by the receiver, allows the use of matched filters or correlation which improves its BER for a given E_b/N_0 (Lathi, 1998).

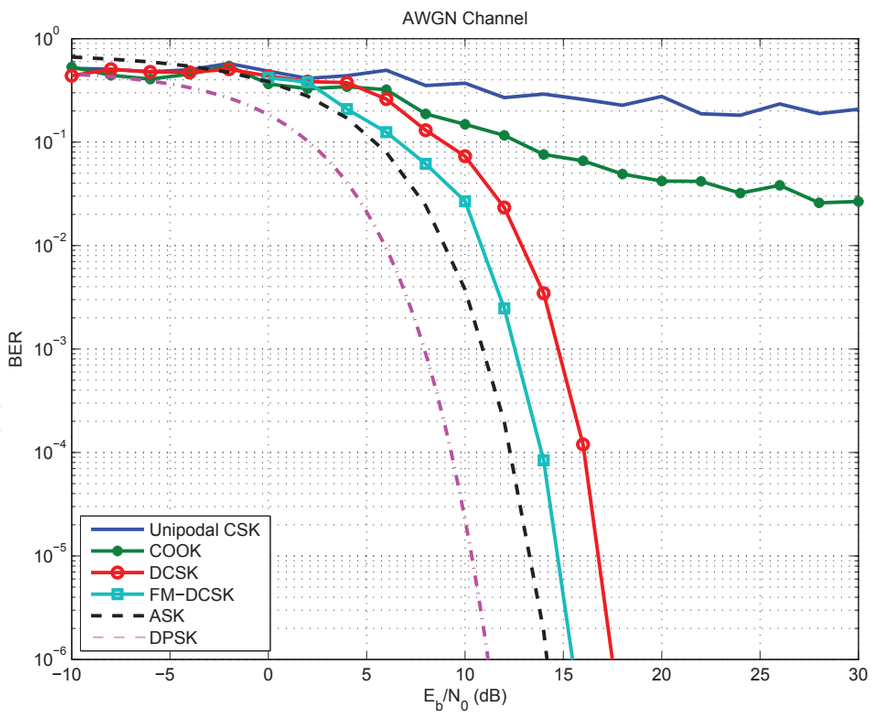

Fig. 7. Symbol error rates in AWGN channel of digital communication systems using chaotic signals for $N = 10$. The curves for conventional Amplitude Shift Keying (ASK) and DPSK are shown for comparison.

Though FM-DCSK has the best features among the analyzed chaotic systems, it is important to note that no information concerning the dynamics of the chaotic map is used in its demodulation. Its performance would be essentially the same in case random sequences were used instead of chaotic ones.
If knowledge of the dynamics of the generator map were used in demodulation process, certainly better results could be obtained, as in conventional systems that use matched filters.

3.4 Chaotic modulations summary

Thus far we presented some of the most studied modulation systems using chaotic signals. Their performance in AWGN channel was qualitatively and quantitatively analyzed.
The discrete-time notation used here is a contribution of this chapter as it is consistent with the maps used in the generation of chaotic signals and also simplifies computational simulations.
Table 1 summarizes the problems encountered in the main digital modulations described. The column **Threshold** concerns the problem of dependence of the decision threshold on the noise power in the channel. The column **Energy** represents the problem of variability of energy per symbol. The column **Sync.** means the need for recovery of basis chaotic functions at the receiver and the last column, **Map Info** when signaled means that the system does not use properties of the chaotic attractor in the estimation of the transmitted symbol.

System	Threshold	Energy	Sync.	Map Info
Coherent CSK		X	X	
Noncoherent CSK	X	X		X
DCSK		X		X
FM-DCSK				X

Table 1. Problems of chaotic modulations studied in the section.

Among the modulations studied, FM-DCSK has the best results because it does not depend on chaotic synchronization, its decision level threshold is independent of noise and it has constant mean energy per symbol.
The analyzed non-coherent and differential receivers have a common feature: they do not use any characteristic of the dynamics of the systems that generate the chaotic signals to process the demodulation. These techniques are limited to estimating characteristics of the received signal and to comparing them to an adequate decision threshold.
A priori knowledge of generating maps by the receiver can be used in two ways:

i. via chaotic synchronization using coherent demodulation or
ii. via improving signal to noise ratio or by distinguishing them through techniques to estimate the chaotic signals arriving at the receiver.

The presence of noise and distortion in the channel brings unsatisfactory results when using chaotic synchronization due to the sensitive dependence on initial conditions that characterize chaotic signals (Kennedy, Setti & Rovatti, 2000; Lau & Tse, 2003; Williams, 2001). Hence the only remaining option is to examine the second alternative.
Some estimation techniques for orbits and initial conditions based on maximizing likelihood functions (Eisencraft et al., 2009; Kisel et al., 2001) have been proposed recently, yielding results better than those presented in this section. The rest of the chapter is devoted to these techniques.

4. Chaotic signal estimation

Assume that an N-point sequence $s'(n)$ is observed whose model is given by

$$s'(n) = s(n) + r(n),\ 0 \leq n \leq N-1, \tag{20}$$

where $s(n)$ is an orbit of the known one-dimensional system

$$s(n) = f(s(n-1)) \tag{21}$$

and $r(n)$ is zero mean AWGN with variance σ^2. The $f(.)$ map is defined over the interval U. The problem is to obtain an estimate $\hat{s}(n)$ of the orbit $s(n)$.
The Cramer-Rao Lower Bound (CRLB), the minimum mean square error that an estimator of the initial condition $s(0)$ can attain, was derived by Eisencraft & Baccalá (2006; 2008).
Let the *estimation gain* G_{dB} in decibels be given by

$$G_{dB} = 10\log\left(\frac{\sigma^2}{e}\right), \tag{22}$$

be the figure of merit, where $e = \overline{(\hat{s}(n) - s(n))^2}$ is the mean square estimation error.
We succinctly review two estimation techniques for noise-embedded chaotic signals: the Maximum Likelihood (ML) Estimator and the Modified Viterbi algorithm (MVA).

4.1 Maximum likelihood estimator

The ML estimator of some scalar parameter θ is the value that maximizes the likelihood function $p(\mathbf{x};\theta)$ for the observation vector $\mathbf{x}$ (Kay, 1993). What motivates this definition is that $p(\mathbf{x};\theta)d\mathbf{x}$ represents the probability of observing $\mathbf{x}$ within a neighborhood given by $d\mathbf{x}$ for some value of θ. In the present context, it was first used by Papadopoulos & Wornell (1993) who show that the estimation gain for an N-point orbit generated by a map with uniform invariant density (Lasota & Mackey, 1985) is limited by

$$G_{dB} \leq 10\log(N+1). \tag{23}$$

which asymptotically corresponds to the Cramer-Rao performance bound.

4.2 Modified Viterbi algorithm

This algorithm is based on that proposed by Dedieu & Kisel (1999) and was generalized for maps with nonuniform invariant density by Eisencraft & do Amaral (2009).
Consider the domain U as the union of disjoint intervals U_j, $j = 1, 2, \ldots, N_S$. At a given instant n, let the signal *state* be $q(n) = j$ if $s(n) \in U_j$. A $(k+1)$-length state sequence is represented by

$$\mathbf{q}_k = [q(0), q(1), \ldots, q(k)]^T \tag{24}$$

and the first $k+1$ observed samples by

$$\mathbf{s}'_k = \left[s'(0), s'(1), \ldots, s'(k)\right]^T. \tag{25}$$

To simplify notation, consider the N-length sequences $\mathbf{q}_{N-1} \equiv \mathbf{q}$ and $\mathbf{s}'_{N-1} \equiv \mathbf{s}'$. Furthermore, the center of interval U_j is denoted by $B(j)$.

Given $\mathbf{s}'$, an estimated state sequence $\hat{\mathbf{q}}$ is sought that maximizes the posterior probability

$$P(\hat{\mathbf{q}}|\mathbf{s}') = \max_{\mathbf{q}} P(\mathbf{q}|\mathbf{s}'). \tag{26}$$

Using Bayes' theorem,

$$P(\mathbf{q}|\mathbf{s}') = \frac{p(\mathbf{s}'|\mathbf{q})P(\mathbf{q})}{p(\mathbf{s}')}, \tag{27}$$

where $p(\mathbf{s}')$ and $p(\mathbf{s}'|\mathbf{q})$ are, respectively, the Probability Density Function (PDF) of $\mathbf{s}'$ and the PDF of $\mathbf{s}'$ given that the state sequence of the signal is $\mathbf{q}$. The probability $P(\mathbf{q})$ is the chance of obtaining the state sequence $\mathbf{q}$ when $f(.)$ is iterated.
Thus, the argument $\hat{\mathbf{q}}$ is such that

$$\hat{\mathbf{q}} = \arg\max_{\mathbf{q}} P(\mathbf{q}|\mathbf{s}') = \arg\max_{\mathbf{q}} p(\mathbf{s}'|\mathbf{q})P(\mathbf{q}). \tag{28}$$

It is important to note that because of the AWGN model and of how signals are generated, $\mathbf{q}_k$ is a first order Markov process where k is the time variable. Thus

$$P\left(\mathbf{q}_k\right) = P\left(q(k)|q(k-1)\right) P\left(\mathbf{q}_{k-1}\right), \tag{29}$$

where $P\left(q(k)|q(k-1)\right)$ is the transition probability from the state $q(k-1)$ to $q(k)$.
Furthermore, taking into account the independence between the noise samples,

$$p(\mathbf{s}'_k|\mathbf{q}_k) = \prod_{n=0}^{k} p\left(s'(n)|q(n)\right) = \prod_{n=0}^{k} p_r(s'(n) - s(n)) \approx \prod_{n=0}^{k} p_r\left(s'(n) - B\left(q(n)\right)\right), \tag{30}$$

with $p_r(.)$ standing for the noise PDF. The approximation in Eq. (30) holds only for sufficiently large N_S.
Using Eqs. (28-30), one can express $P(\mathbf{q}|\mathbf{s}')$ as a product of state transition probabilities by conditional observation probabilities. Hence $\hat{\mathbf{q}}$ is the sequence that maximizes

$$\left(\prod_{n=1}^{N-1} P\left(q(n)|q(n-1)\right) p\left(s'(n)|q(n)\right)\right) P\left(q(0)\right). \tag{31}$$

Choosing the partition $U_j, j = 1, 2, \ldots, N_S$ so that the probability of each possible state $q(n) = j$ is the same for all j, the last term in Eq. (31), $P\left(q(0)\right)$, can be eliminated leading to

$$\hat{\mathbf{q}} = \arg\max_{\mathbf{q}} \prod_{n=1}^{N-1} P\left(q(n)|q(n-1)\right) p\left(s'(n)|q(n)\right), \tag{32}$$

as in (Kisel et al., 2001). Note, however, the central role played by the choice of the partition in obtaining this result as recently pointed out by Eisencraft et al. (2009).
Finding $\mathbf{q}$ that maximizes the product in Eq. (32) is a classic problem whose efficient solution is given by the Viterbi Algorithm (Forney, 1973; Viterbi, 1967), which was first applied to the estimation of chaotic signals by Marteau & Abarbanel (1991). The main advantage in its use lies in dispensing with exhaustive search on the $(N_S)^N$ possible state sequences for an N-point signal.
Let $\gamma(n, j)$ be the probability of the most probable state sequence, in the maximum likelihood sense, that ends in state j, at instant $n \geq 1$, given the observed sequence $\mathbf{s}'$, or

$$\gamma(n, j) = \max_{\mathbf{q}_n} P(\mathbf{q}_{n-1}, q(n) = j|\mathbf{s}'). \tag{33}$$

Using Eqs. (29-30), $\gamma(n,j)$ can be calculated recursively

$$\gamma(n,j) = \max_i \left[\gamma(n-1,i)a_{ij}\right] b_j\left(s'(n)\right), \tag{34}$$

for $n > 1$ where

$$a_{ij} = P\left(q(n) = j | q(n-1) = i\right) \tag{35}$$

and

$$b_j\left(s'(n)\right) = p\left(s'(n) | q(n) = j\right). \tag{36}$$

The coefficients a_{ij} are the state transition probabilities that depend on the map $f(.)$ and on the partition. Let the transition probability matrix be given by

$$\mathbf{A}_{N_S \times N_S} = a_{ij}, 1 \leq i,j \leq N_S. \tag{37}$$

The $b_j(.)$ coefficients represent the observation conditional probabilities that depend only on the noise PDF $p_r(.)$.
The Viterbi algorithm proceeds in two passes, the forward one and the backward one:

- **Forward pass**: for each instant $1 \leq n \leq N-1$, Eqs. (33 - 34) are used to calculate $\gamma(n,j)$ for the N_S states. Among the N_S paths that can link states $j = 1,\ldots,N_S$ at instant $n-1$ to state j at instant n, only the most probable one is maintained. The matrix $\varphi(n,j)$, $n = 1,\ldots,N-1$, $j = 1,\ldots,N_S$, stores the state at instant $n-1$ that takes to state j with maximal probability. In the end of this step, at instant $n = N-1$, we select the most probable state as $\hat{q}(N-1)$.
- **Backward pass**: for obtaining the most probable sequence, it is necessary to consider the argument i that maximizes Eq. (34) for each n and j. This is done defining

$$\hat{q}(n) = \varphi\left(n+1, \hat{q}(n+1)\right), \; n = N-2,\ldots,0. \tag{38}$$

Once obtained $\hat{q}(n)$, the estimated orbit is given by the centers of the subintervals related to the most probable state sequence,

$$\hat{s}(n) = B\left(\hat{q}(n)\right), \; n = 0,\ldots,N-1. \tag{39}$$

4.2.1 Partition of the state space

To apply the algorithm one must choose a partition so that the probability of an orbit point to be in any state is the same, to eliminate $P\left(q(0)\right)$ in Eq. (31). This means that if a given map has invariant density $p(s)$ (Lasota & Mackey, 1985), one should take N_S intervals $U_j = [u_j; u_{j+1}]$ so that, for every $j = 1,\ldots,N_S$,

$$\int_{u_j}^{u_{j+1}} p(s)ds = \frac{1}{N_S}. \tag{40}$$

Using the ergodicity of chaotic orbits (Lasota & Mackey, 1985), it is possible to estimate $p(s)$ for a given $f(.)$ and thereby obtain the correct partition.
The maps taken as examples by Xiaofeng et al. (2004) and Kisel et al. (2001) have uniform invariant density and the authors proposed using equal length subintervals. However, this choice is not applicable to arbitrary one-dimensional maps. When using Viterbi algorithm with the correct partition, it is called here *Modified Viterbi Algorithm* (MVA) (Eisencraft et al., 2009).

As illustrative examples, consider the uniform invariant density tent map defined in $U = (-1, 1)$ as Eq.(6) and the nonuniform invariant density quadratic map

$$f_Q(s) = 1 - 2s^2, \tag{41}$$

defined over the same U (Eisencraft & Baccalá, 2008). It can be shown (Lasota & Mackey, 1985) that, the invariant density of these maps are

$$p_T(s) = 1/2 \tag{42}$$

and

$$p_Q(s) = \frac{1}{\pi\sqrt{1 - s^2}}, \tag{43}$$

respectively.
An example of orbit for each of these maps and their respective invariant densities are shown in Figures 8 and 9. The partition satisfying Eq. (40) for each case is also indicated when $N_S = 5$.

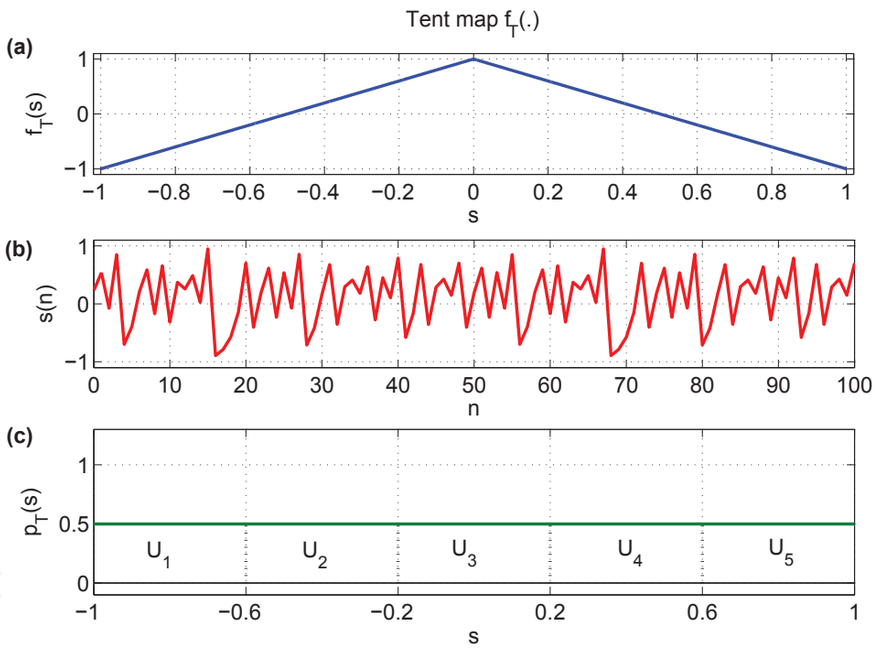

Fig. 8. (a) Tent map $f_T(.)$; (b) example of a 100-point signal generated by $f_T(.)$; (c) invariant density along with the partition satisfying Eq. (40) for $N_S = 5$.

Figures 10 and 11 present how the performance of MVA varies for different values of N_S and $N = 10$. In Figure 10 the generating map is $f_T(.)$ whereas $f_Q(.)$ is used in Figure 11. To illustrate the importance of the correct partition choice, Figure 11(a) displays the results of mistakenly using a uniform partition whereas Figure 11(b) displays the results of using the correct partition according to Eq. (40). The input and output SNR are defined as

$$\text{SNR}_{\text{in}} = \frac{\sum_{n=0}^{N-1} s^2(n)}{N\sigma^2} \tag{44}$$

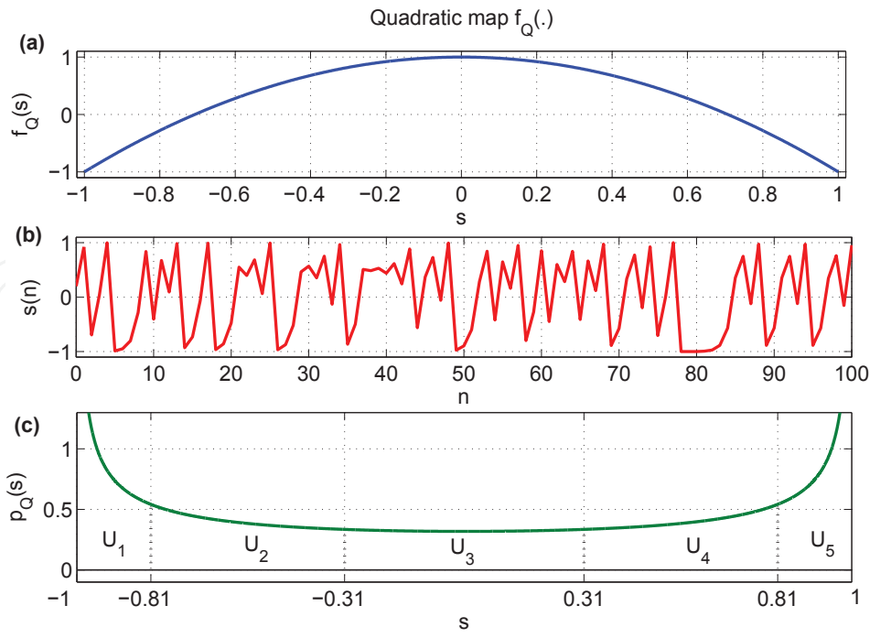

Fig. 9. (a) Quadratic map $f_Q(.)$; (b) example of a 100-point signal generated by $f_Q(.)$; (c) invariant density along with the partition satisfying Eq. (40) for $N_S = 5$.

and

$$\mathrm{SNR}_{\mathrm{out}} = \frac{\sum_{n=0}^{N-1} s^2(n)}{\sum_{n=0}^{N-1} \left(s(n) - \hat{s}(n)\right)^2}. \tag{45}$$

For each $\mathrm{SNR}_{\mathrm{in}}$ of the input sequence, the average $\mathrm{SNR}_{\mathrm{out}}$ of 1000 estimates is shown.
Choosing the right partition, the estimation algorithm has an increasing performance as a function of $\mathrm{SNR}_{\mathrm{in}}$ until $\mathrm{SNR}_{\mathrm{out}}$ attains a limit value which depends on N_S. This limiting value can be calculated assuming that, in the best possible case, the estimation error is caused by domain quantization alone. As such, for an uniform partition, the estimation error is an uniformly distributed random variable in the interval $[-1/N_S, 1/N_S]$. Therefore the mean squared value of $s(n) - \hat{s}(n)$ is limited by $1/\left(3N_S^2\right)$. Additionally, $s(n)$ is uniformly distributed in $[-1, 1]$ and, consequently, has a mean squared value of $1/3$. Hence if all the points are in the correct subintervals, the expected value of $\mathrm{SNR}_{\mathrm{out}}$, $E[\mathrm{SNR}_{\mathrm{out}}]$ in dB is

$$E\left[\mathrm{SNR}_{\mathrm{out}}\right] = E\left[10\log\frac{\sum_{n=0}^{N-1} s^2(n)}{\sum_{n=0}^{N-1}(s(n) - \hat{s}(n))^2}\right] = 10\log\frac{N/3}{N/(3N_S^2)} = 20\log N_S. \tag{46}$$

These limits, which are exact only in the uniform partition case, are indicated with dashed lines for each N_S value in Figures 10 and 11.
Comparing Figures 11(a) and (b) reveals the critical role played by the partition choice. Clearly the uniform partition of Xiaofeng et al. (2004) and Kisel et al. (2001) cannot attain the best possible $\mathrm{SNR}_{\mathrm{out}}$ for the quadratic map whose invariant density is not uniform.
Figures 10 and 11(b) show that the algorithm has slightly better performance for the quadratic map. This result confirms the importance of map choice.

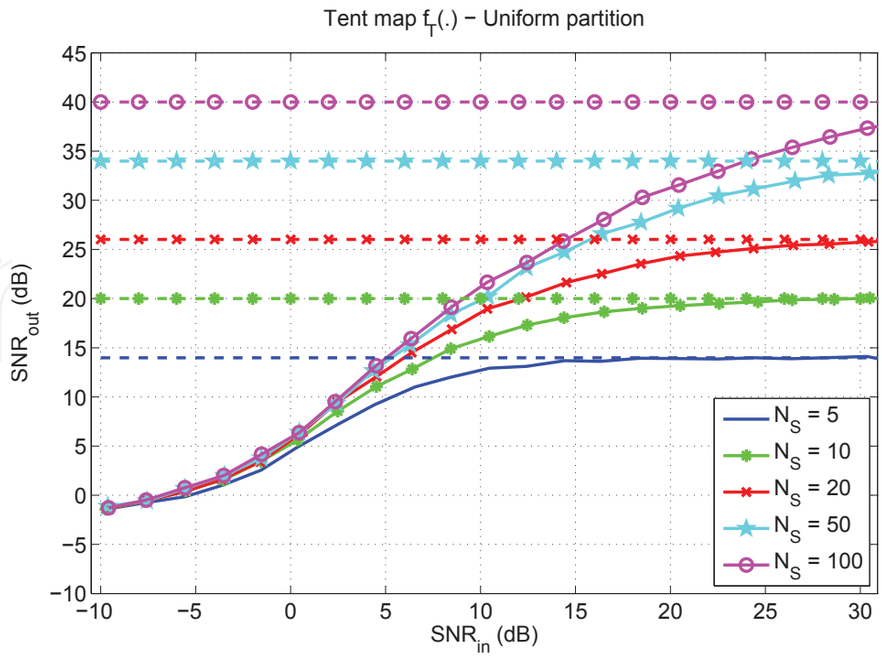

Fig. 10. $\mathrm{SNR}_{\mathrm{out}}$ of MVA for an orbit of length $N = 10$ using different numbers of partition intervals N_S . The generating map is $f_T(.)$. Performance limits of Eq. (46) are indicated by dashed lines.

4.3 Comparing MVA and MLE

MLE's performance is strongly influenced by the length of the estimated orbit N, as shown by inequality (23). MVA is more sensitive to the number of subsets N_S used in the partition. Simulations show that the gain obtained via MLE monotonically increases with Signal to Noise Ratio (SNR) being bounded by the CRLB. Using MVA, the gain attains a maximum value and decays and even becomes negative (in dB) due to quantization error. So the N_S choice is a very important concern for MVA and it is a function of the expected SNR.

The estimation gain for both methods on tent map orbits from Eq. (6) corrupted by AWGN is shown in Figure 12. For the MVA only the $N = 20$ result is depicted as simulations show little improvement for larger N.

From Figure 12 one can see that for SNR $\leq$ 20dB, which is the usual operating range, MVA's performance is superior.

These results, plus the fact that MVA can be simply applied to broader map classes have induced the choice of MVA in the communication applications described next.

5. Chaotic signal estimation applied to communication

In this section we propose two binary digital modulation using chaotic system identification. They are the *Modified Maximum Likelihood Chaos Shift Keying* (MMLCSK) using one and two maps. Both are based on the ones proposed by Kisel et al. (2001). We have modified them using nonuniform partitions for the MVA as discussed in the previous section. In this way, it is possible to test the performance of nonuniform invariant density maps.

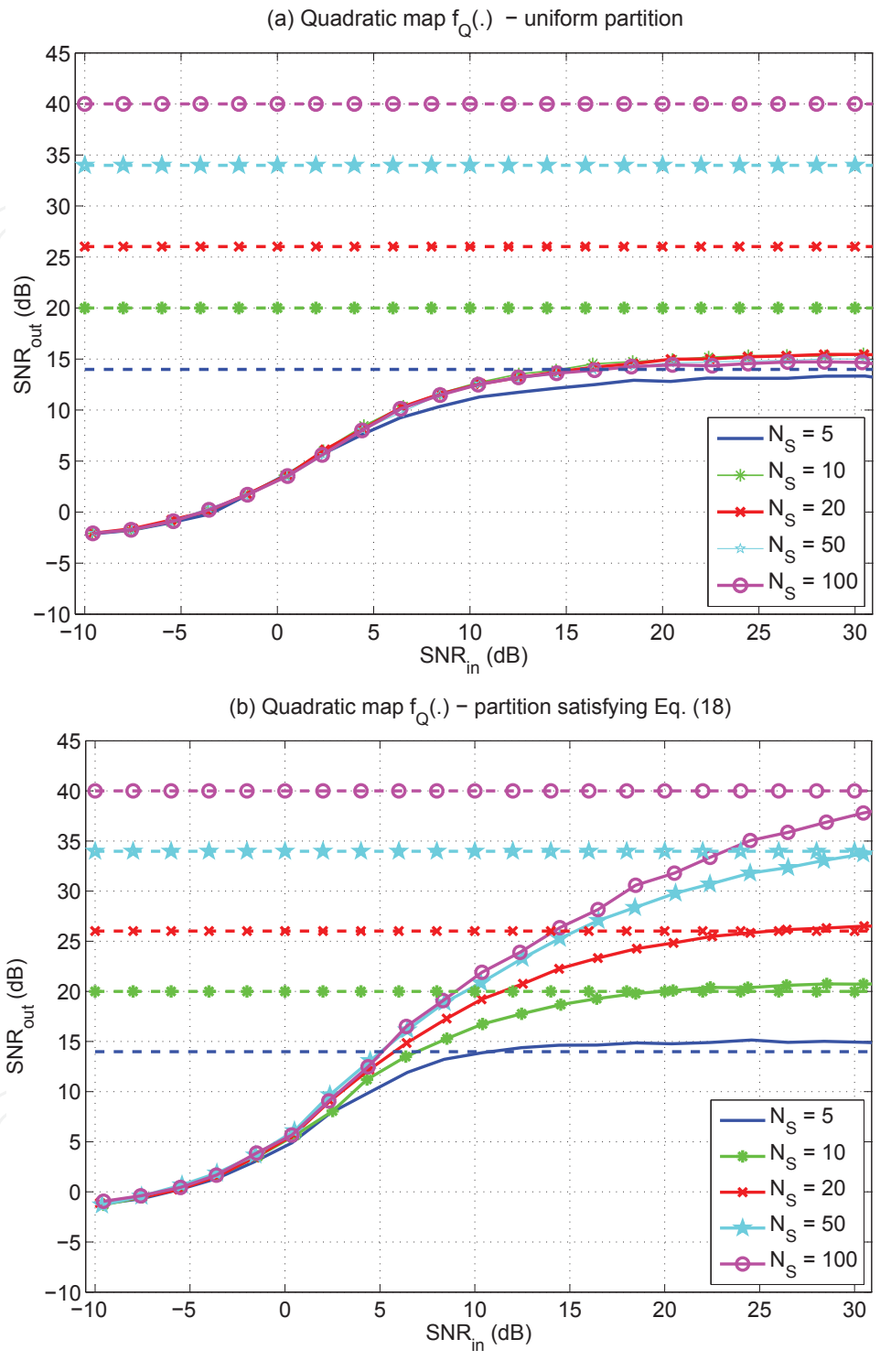

Fig. 11. $\mathrm{SNR}_{\mathrm{out}}$ of the MVA for an orbit of length $N = 10$ using different number of partition intervals N_S. The generating map is $f_Q(.)$. Results for an uniform partition (a) are contrasted to the improved values in (b) using a partition satisfying Eq. (40). Limits of Eq. (46) are indicated by dashed lines.

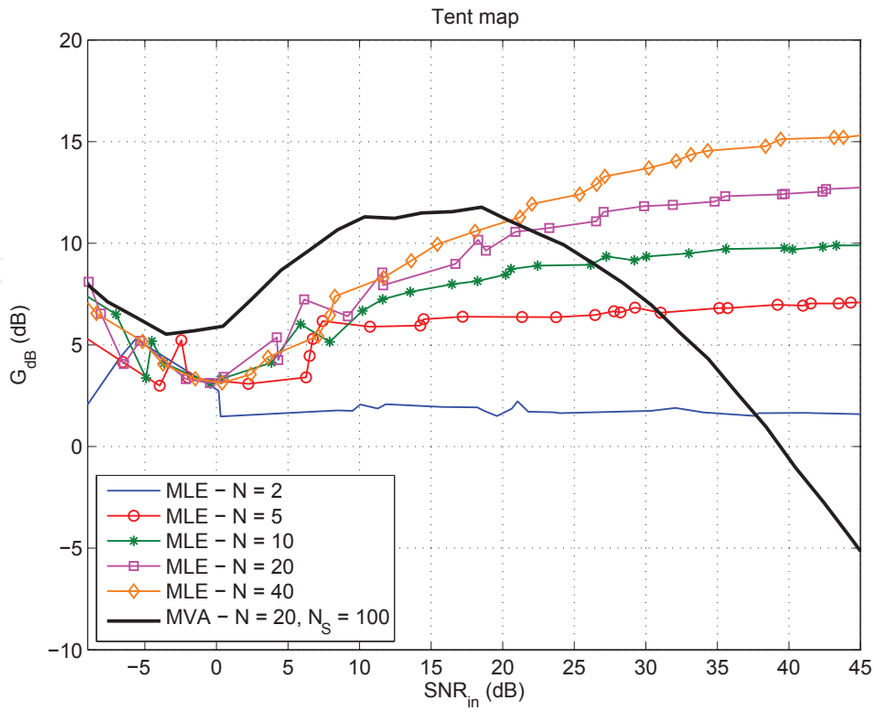

Fig. 12. Estimation gain for MLE and MVA for tent map Eq. (6).

5.1 MMLCSK using two maps

In this case, each symbol is associated with a different map, $f_1(.)$ or $f_2(.)$. To transmit a "0", the transmitter sends an N-point orbit $s_1(.)$ of $f_1(.)$ and to transmit a "1" it sends an N-point orbit $s_2(.)$ of $f_2(.)$.

Maps must be chosen so that their state transition probabilities matrix (Eq. (37)) $\mathbf{A}_1$ and $\mathbf{A}_2$ are different. Estimating $s_1(n)$ using MVA with $\mathbf{A}_2$ must produce a small estimation gain or even a negative (in dB) one. The same must happen when we try to estimate $s_2(n)$ using $\mathbf{A}_1$.

The receiver for MMLCSK using two maps is shown in Figure 13. The Viterbi decoders try to estimate the original $s(n)$ using $\mathbf{A}_1$ or $\mathbf{A}_2$. For each symbol, the estimated state sequences are $\hat{\mathbf{q}}_1$ and $\hat{\mathbf{q}}_2$.

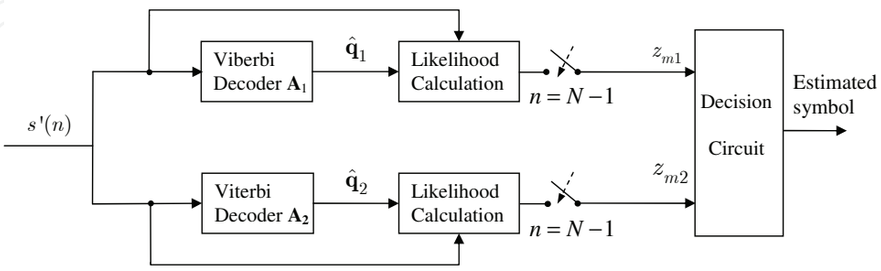

Fig. 13. Receiver for MMLCSK using two maps.

Given the observed samples, z_{m1} e z_{m2} are proportional to the probability of obtaining $\hat{\mathbf{q}}_1$ and $\hat{\mathbf{q}}_2$ respectively. More precisely,

$$z_{m1} = \prod_{n=1}^{N-1} P(\hat{q_1}(n)|\hat{q}_1(n-1), \mathbf{A}_1) p(s'(n)|\hat{q_1}(n)), \tag{47}$$

$$z_{m2} = \prod_{n=1}^{N-1} P(\hat{q_2}(n)|\hat{q}_2(n-1), \mathbf{A}_2) p(s'(n)|\hat{q_2}(n)). \tag{48}$$

In these equations the likelihood measure of Eq. (32) was used. The probability $P(\hat{q}(n)|\hat{q}(n-1), \mathbf{A}_i)$ can be read directly from $\mathbf{A}_i$ and $p(x'(n)|\hat{q}(n))$ depends only on the noise and can be approximated as described by Dedieu & Kisel (1999).
Choosing the largest between z_{m1} e z_{m2} allows *identifying* the map used in the transmitter with maximum likelihood and thereby decode the transmitted symbol.
Given some $f_1(.)$ map, an important problem is to find the matching $f_2(.)$ map so that its probability transition matrix $\mathbf{A}_2$ permits optimal discrimination between the likelihood measures of Eqs. (47) and (48). For piecewise linear maps on the interval $U = [-1, 1]$ we can use the following rule adapted from (Kisel et al., 2001):

$$f_2(s) = \begin{cases} f_1(s) + 1, \, f_1(s) < 0 \\ f_1(s) - 1, \, f_1(s) \geq 0 \end{cases}. \tag{49}$$

Figure 14(a) shows the construction of map $f_2(.)$ from $f_1(.) = f_T(.)$. This way, $f_1(s)$ and $f_2(s)$ map a point s a unity away.
In this case, using an uniform partition for $N_S = 5$ we have

$$\mathbf{A}_1 = \begin{bmatrix} 1/2 & 1/2 & 0 & 0 & 0 \\ 0 & 0 & 1/2 & 1/2 & 0 \\ 0 & 0 & 0 & 0 & 1 \\ 0 & 0 & 1/2 & 1/2 & 0 \\ 1/2 & 1/2 & 0 & 0 & 0 \end{bmatrix}, \mathbf{A}_2 = \begin{bmatrix} 0 & 0 & 1/3 & 1/3 & 1/3 \\ 1/3 & 1/3 & 0 & 0 & 1/3 \\ 0 & 1/2 & 1/2 & 0 & 0 \\ 1/3 & 1/3 & 0 & 0 & 1/3 \\ 0 & 0 & 1/3 & 1/3 & 1/3 \end{bmatrix}. \tag{50}$$

It can be shown that almost every orbit generated by $f_2(.)$ is in fact chaotic (Kisel et al., 2001). Note however that this method is not necessarily optimal and must be used prudently. There is no guarantee that the orbits of $f_2(.)$ given by Eq. (49) are chaotic in general.
For instance, if we apply the same strategy for the quadratic map $f_1(s) = f_Q(s)$ from Eq. (41), we obtain $f_2(s)$ show in Figure 14(b). All the orbits of $f_2(.)$ converge to a stable fixed point at $s = 0$ and hence are not chaotic at all (Alligood et al., 1997).
In the simulations presented here $f_2(.) = -f_Q(.)$ as shown in Figure 14(c). This map is possibly not optimum because points next to the roots of $f_1(.)$ and $f_2(.)$ are mapped near to each other by both functions. The transition matrix for these two maps for $N_S = 5$ using the partition obeying Eq. (40) are

$$\mathbf{A}_1 = \begin{bmatrix} 1/2 & 1/2 & 0 & 0 & 0 \\ 0 & 0 & 1/2 & 1/2 & 0 \\ 0 & 0 & 0 & 0 & 1 \\ 0 & 0 & 1/2 & 1/2 & 0 \\ 1/2 & 1/2 & 0 & 0 & 0 \end{bmatrix}, \; \mathbf{A}_2 = \begin{bmatrix} 0 & 0 & 0 & 1/2 & 1/2 \\ 0 & 0 & 1 & 0 & 0 \\ 1 & 0 & 0 & 0 & 0 \\ 0 & 0 & 1 & 0 & 0 \\ 0 & 0 & 0 & 1/2 & 1/2 \end{bmatrix}. \tag{51}$$

In this case, it can be shown that $f_2(.)$ generates chaotic orbits (Alligood et al., 1997). However, note that a_{23} and a_{43} exhibit nonzero probabilities in both matrices that will probably generate

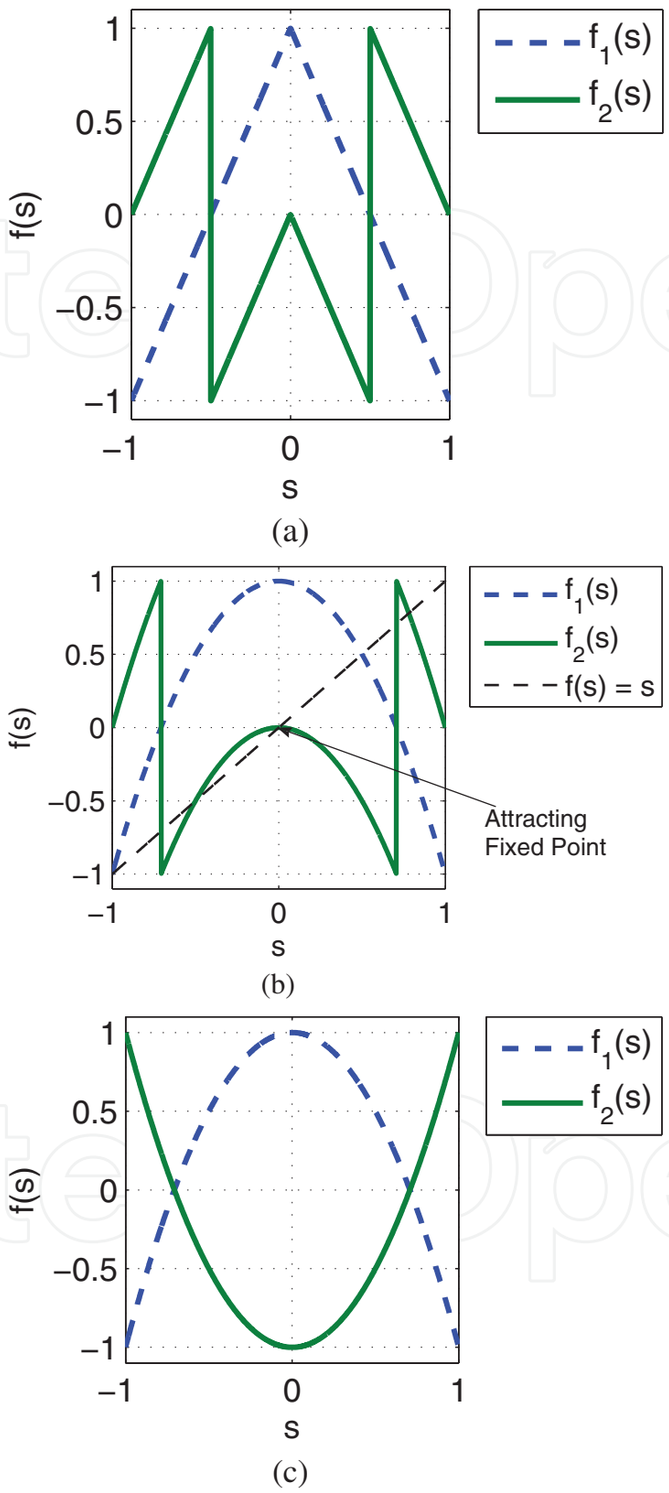

Fig. 14. (a) Construction of map $f_2(.)$ for $f_1(.) = f_T(.)$ using Eq. (49); (b) construction of $f_2(.)$ for $f_1(.) = f_Q(.)$ using Eq. (49). Note the attracting fixed point; (c) construction of $f_2(.)$ for $f_1(.) = f_Q(.)$ used in simulations.

errors in the MMLCSK receiver. As such this pair of maps is expected to have worse performance when compared to the one with matrices given by Eq. (50).
To find $f_2(.)$ given a map $f_1(.)$ that presents optimal properties when it comes to identification through matrices $\mathbf{A}_1$ and $\mathbf{A}_2$ is an open problem. As shown by the last example, it is necessary to impose that $f_2(.)$ generates chaotic orbits.
Figure 15 shows examples of transmitted MMLCSK using two maps for $f_1(.) = f_T(.)$ and $f_1(.) = f_Q(.)$.

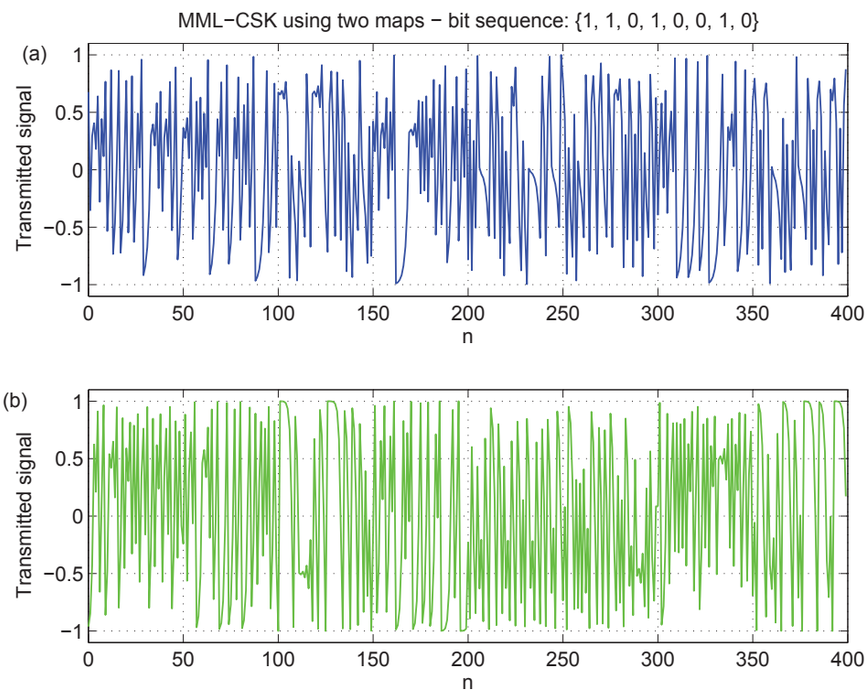

Fig. 15. MML-CSK signals using two maps for the bit sequence $\{1,1,0,1,0,0,1,0\}$: (a) $f_T(.)$; (b) $f_Q(.)$. In both cases, 50 samples per bit are used.

5.2 MMLCK using one map

As an alternative, it is possible to construct a communication system based on MVA estimation using just one map. In this case, according to the symbol that is intended to be communicated, the chaotic signal is directly transmitted or an invertible transformation is applied on the sequence. This operation must modify the sequence so that it is no longer a valid orbit of the map which dispenses with finding an $f_2(.)$ map.
In the binary case, for maps that are not odd, this transformation can be, for instance, $T(s) = -s$ which can be undone by multiplying the sequence by -1. To transmit a **0**, an N-point orbit $s_1(.)$ of $f_1(.)$ is sent. To transmit a **1** is sent $-s_1(.)$.
The receiver for this system is shown in Figure 16. The variables z_{m1} and z_{m2} are calculated by Eq. (47). However, when calculating z_{m2}, $s'(n)$ is substituted by $-s'(n)$. So, when a **0** is received, the likelihood expressed by z_{m1} must be greater than z_{m2} because $-s_1(n)$ is not an orbit of $f_1(.)$. The opposite is true when a **1** is received.
It is relevant to note that this scheme can be easily generalized to M-ary modulation, $M > 2$. For this all that is needed is to consider other invertible transformations.

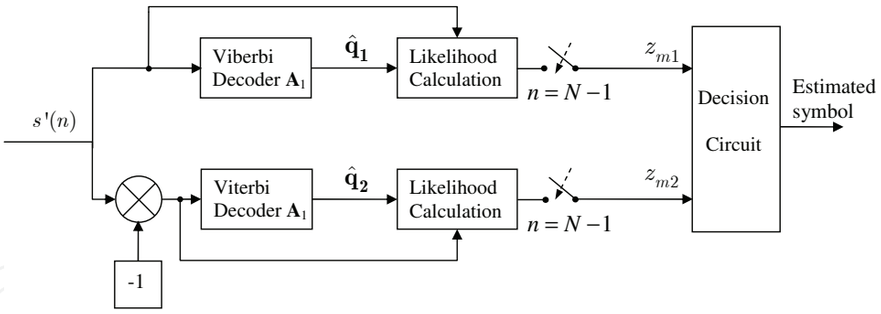

Fig. 16. Receiver for MMLCSK using one maps.

Figure 17 shows examples of modulated signals using one map for $f_1(.) = f_T(.)$ and $f_1(.) = f_Q(.)$.

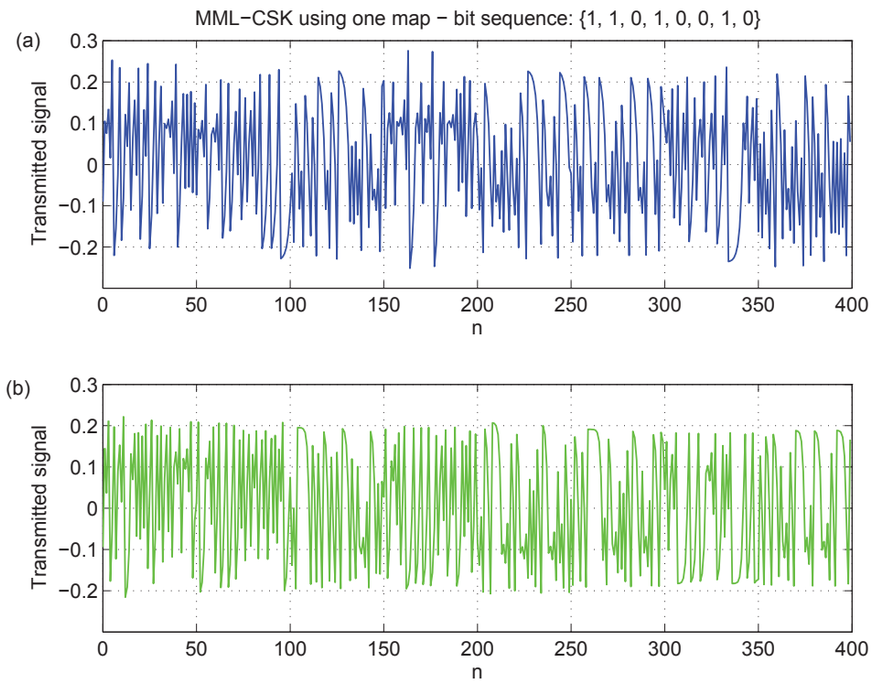

Fig. 17. MML-CSK signals using one map for the bit sequence $\{1,1,0,1,0,0,1,0\}$: (a) $f_T(.)$; (b) $f_Q(.)$. In both cases, 50 samples per bit are used.

5.3 Numerical simulations

Figure 18 shows the BER as a function of the bit energy per power spectral density of the AWGN (E_b/N_0) for the MMLCSK using one and two maps. In the estimation and identification process $N_S = 100$ subsets and $N = 50$ samples per bit were used. For the sake of comparison, the performance of Chaos On-Off Keying (COOK) (the best performing non-coherent chaos communication system that does not use estimation) is also shown (Kolumban, Kennedy & Chua, 1998). COOK uses only bit energy estimation to decode the signal. MMLCSK performs much better than COOK. The attained BER, however, is still far from that of conventional Amplitude Shift Keying (ASK).

Our simulations show that MMLCSK using one map has slightly better performance than MMLCSK using two maps. Besides $f_T(.)$ performs better than $f_Q(.)$. This last results confirms the importance of both map choice and transformation.

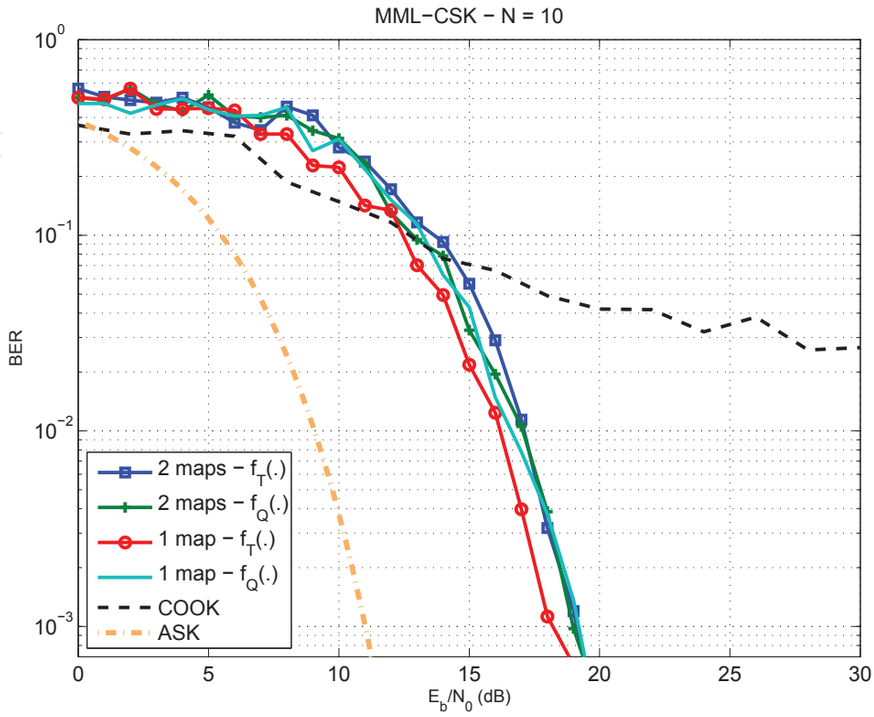

Fig. 18. Bit Error Rate (BER) for the tested MMLCSK modulations. Each bit was represented by $N = 10$ samples.

6. Conclusions

In this chapter we reviewed some chaos-based digital communication systems and studied their performance in a noisy environment.

In Section 3 we described CSK, DCSK and FM-DCSK using a discrete-time low-pass unifying notation. We concluded that FM-DCSK has the best performance among them. However the BER it attains in an AWGN channel is still unsatisfactory compared to conventional systems. This occurs mainly because FM-DCSK does not use any characteristic of the system that generate the chaotic signals to process the demodulation.

One possible way for improvement is to use estimation techniques to increase the SNR at the receiver. We review two such estimation techniques in Section 4, MLE and MVA. Due to its superior characteristics, we used the latter to propose two binary digital modulation schemes using chaotic signal estimation. Despite presenting better BER performance than the previous proposals, chaos based modulations still have a long way to go before they can attain the same performance level of conventional systems and so become practical options in noisy environments.

7. References

Alligood, K. T., Sauer, T. D. & Yorke, J. A. (1997). *Chaos: An Introduction to Dynamical Systems*, Textbooks In Mathematical Sciences, Springer-Verlag, New York.

Argyris, A., Syvridis, D., Larger, L., Annovazzi-Lodi, V., Colet, P., Fischer, I., Garcia-Ojalvo, J., Mirasso, C., Pesquera, L. & Shore, K. (2005). Chaos-based communications at high bit rates using commercial fibre-optic links, *Nature* 438(7066): 343–346.

Dedieu, H. & Kisel, A. (1999). Communications with chaotic time series: probabilistic methods for noise reduction, *International Journal of Circuit Theory and Applications* 27(6): 577–587.

Djurovic, I. & Rubezic, V. (2008). Chaos detection in chaotic systems with large number of components in spectral domain, *Signal Processing* 88(9): 2357 – 2362.

Eisencraft, M. & Baccalá, L. A. (2006). Estimating the initial conditions of chaotic orbits: performance bounds, *Proc. 1st IFAC Conference on Analysis and Control of Chaotic Systems*, Reims, France, pp. 291–295.

Eisencraft, M. & Baccalá, L. A. (2008). The Cramer-Rao Bound for initial conditions estimation of chaotic orbits, *Chaos Solitons & Fractals* 38(1): 132–139.

Eisencraft, M. & do Amaral, M. A. (2009). Estimation of nonuniform invariant density chaotic signals with applications in communications, *Second IFAC meeting related to analysis and control of chaotic systems*, London, England, pp. 1–6.

Eisencraft, M., do Amaral, M. A. & Lima, C. A. M. (2009). Estimation of chaotic signals with applications in communications, *Proc. 15th IFAC Symposium on System Identification*, Saint-Malo, France, pp. 1–6.

Eisencraft, M., Kato, D. M. & Monteiro, L. H. A. (2010). Spectral properties of chaotic signals generated by the skew tent map

Endo, T. & Chua, L. (1988). Chaos from phase-locked loops, *IEEE Transactions on Circuits and Systems* 35(8): 987–1003.

Forney, G. D. (1973). Forney, G. D. (1973). The Viterbi algorithm, *IProceedings of the IEEE* 61(3): 268 - 278.

Harb, B. A. & Harb, A. M. (2004). Chaos and bifurcation in a third-order phase locked loop, *Chaos, Solitons & Fractals* 19(3): 667 – 672.

Haykin, S. S. (2000). *Communication systems*, fourth edn, Wiley, New York.

Kaddoum, G., Charge, P., Roviras, D. & Fournier-Prunaret, D. (2009). A Methodology for Bit Error Rate Prediction in Chaos-based Communication Systems, *Circuits Systems and Signal Processing* 28(6): 925–944.

Kay, S. M. (1993). *Fundamentals of statistical signal processing: estimation theory*, Prentice-Hall, Inc., Upper Saddle River, NJ, USA.

Kennedy, M. & Kolumban, G. (2000). Digital communications using chaos, *Signal Processing* 80(7): 1307–1320.

Kennedy, M. P., Kolumbán, G., Kis, G. & Jákó, Z. (2000). Performance evaluation of FM-DCSK modulation in multipath enviromnments, 47(12): 1702–1711.

Kennedy, M. P., Setti, G. & Rovatti, R. (eds) (2000). *Chaotic Electronics in Telecommunications*, CRC Press, Inc., Boca Raton, FL, USA.

Kisel, A., Dedieu, H. & Schimming, T. (2001). Maximum likelihood approaches for noncoherent communications with chaotic carriers, *Circuits and Systems I: Fundamental Theory and Applications, IEEE Transactions on* 48(5): 533–542.

Kolumban, G., Kennedy, M. & Chua, L. (1997). The role of synchronization in digital communications using chaos. I . fundamentals of digital communications, 44(10): 927–936.

Kolumban, G., Kennedy, M. & Chua, L. (1998). The role of synchronization in digital communications using chaos. II. chaotic modulation and chaotic synchronization, 45(11): 1129–1140.

Kolumbán, G., P.Kennedy, M., Kis, G. & Jákó, Z. (1998). FM-DCSK: a novel method for chaotic communications, *Proc. ISCAS'98*, Vol. 4, Monterey, USA, pp. 477–480.

Lasota, A. & Mackey, M. (1985). *Probabilistic Properties of Deterministic Systems*, Cambridge University Press, Cambridge.

Lathi, B. P. (1998). *Modern Digital and Analog Communication Systems*, 3.ed edn, Oxford University Press, Inc., New York, NY, USA.

Lau, F. C. M. & Tse, C. K. (2003). *Chaos-based digital communication systems*, Springer, Berlin.

Marteau, F. F. & Abarbanel, H. D. I. (1991). Noise reduction in chaotic time series using scaled probabilistic method, *Jornal of Nonlinear Science* 1(3): 313–343.

Monteiro, L. H. A., Lisboa, A. C. & Eisencraft, M. (2009). Route to chaos in a third-order phase-locked loop network, *Signal Processing* 89(8): 1678–1682.

Papadopoulos, H. & Wornell, G. (1993). Optimal detection of a class of chaotic signals, *Acoustics, Speech, and Signal Processing, 1993. ICASSP-93., 1993 IEEE International Conference on* 3: 117–120 vol.3.

Pecora, L. & Carroll, T. (1990). Synchronization in chaotic systems, *Physical Review Letters* 64(8): 821–824.

Stavroulakis, P. (ed.) (2005). *Chaos Applications in Telecommunications*, CRC Press, Inc., Boca Raton, FL, USA.

Strogatz, S. H. (2001). *Nonlinear Dynamics and Chaos: with Applications to Physics, Biology, Chemistry and Engineering*, Perseus Books Group.

Syvridis, D. (2009). Optical Chaos Encoded Communications: Solutions for Today and Tomorrow, *2009 IEEE LEOS Annual Meeting Conference Proceedings, Vols 1and 2*, IEEE Lasers and Electro-Optics Society (LEOS) Annual Meeting, IEEE Photon Soc, IEEE, pp. 759–760.

Tavazoei, M. S. & Haeri, M. (2009). Chaos in the APFM nonlinear adaptive filter, *Signal Processing* 89(5): 697 – 702.

Tsekeridou, S., Solachidis, V., Nikolaidis, N., Nikolaidis, A., Tefas, A. & Pitas, I. (2001). Statistical analysis of a watermarking system based on Bernoulli chaotic sequences, *Signal Processing* 81(6): 1273–1293.

Viterbi, A. J. (1967). Error bounds for convolutional codes and an asymptotically optimum decoding algorithm, *Information Theory, IEEE Transactions on* 13(2): 260–269.

Williams, C. (2001). Chaotic communications over radio channels, *Circuits and Systems I: Fundamental Theory and Applications, IEEE Transactions on* 48(12): 1394 –1404.

Wozencraft, J. M. & Jacobs, I. M. (1987). *Principles of Communication Engineering*, Wiley, New York, NY, USA.

Xiaofeng, G., Xingang, W. & Meng, Z. (2004). Chaotic digital communication by encoding initial conditions, *Chaos* 14(2): 358–363.

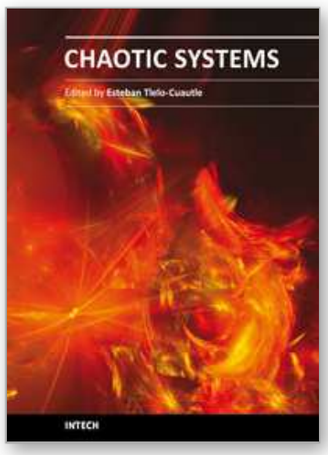

Chaotic Systems

Edited by Prof. Esteban Tlelo-Cuautle

ISBN 978-953-307-564-8
Hard cover, 310 pages
Publisher InTech
Published online 14, February, 2011
Published in print edition February, 2011

This book presents a collection of major developments in chaos systems covering aspects on chaotic behavioral modeling and simulation, control and synchronization of chaos systems, and applications like secure communications. It is a good source to acquire recent knowledge and ideas for future research on chaos systems and to develop experiments applied to real life problems. That way, this book is very interesting for students, academia and industry since the collected chapters provide a rich cocktail while balancing theory and applications.

How to reference

In order to correctly reference this scholarly work, feel free to copy and paste the following:

Marcio Eisencraft and Luiz Antonio Baccalá (2011). Applying Estimation Techniques to Chaos-Based Digital Communications, Chaotic Systems, Prof. Esteban Tlelo-Cuautle (Ed.), ISBN: 978-953-307-564-8, InTech, Available from: http://www.intechopen.com/books/chaotic-systems/applying-estimation-techniques-to-chaos-based-digital-communications

INTECH
open science | open minds

InTech Europe
University Campus STeP Ri
Slavka Krautzeka 83/A
51000 Rijeka, Croatia
Phone: +385 (51) 770 447
Fax: +385 (51) 686 166
www.intechopen.com

InTech China
Unit 405, Office Block, Hotel Equatorial Shanghai
No.65, Yan An Road (West), Shanghai, 200040, China
中国上海市延安西路65号上海国际贵都大饭店办公楼405单元
Phone: +86-21-62489820
Fax: +86-21-62489821

IntechOpen